

Flow along a diverging channel

By **S. C. R. DENNIS**¹, **W. H. H. BANKS**²,
P. G. DRAZIN² AND **M. B. ZATURSKA**²

¹Department of Applied Mathematics, University of Western Ontario, London, Ontario,
Canada N6A 5B9
e-mail: 1003_463@uwovax.uwo.ca

²School of Mathematics, University of Bristol, Bristol BS8 1TW, UK
e-mail: W.Banks@bris.ac.uk; P.Drazin@bris.ac.uk; M.Zaturaska@bris.ac.uk

(Received 27 February 1995 and in revised form 29 October 1996)

This paper treats the two-dimensional steady flow of a viscous incompressible fluid driven through a channel bounded by two walls which are the radii of a sector and two arcs (the ‘inlet’ and ‘outlet’), with the same centre as the sector, at which inflow and outflow conditions are imposed. The computed flows are related to both a laboratory experiment and recent calculations of the linearized ‘spatial’ modes of Jeffery–Hamel flows. The computations, at a few values of the angle between the walls of the sector and several values of the Reynolds number, show how the first bifurcation of the flow in a channel is related to spatial instability. They also show how the end effects due to conditions at the inlet and outlet of the channel are related to the spatial modes: in particular, Saint-Venant’s principle breaks down when the flow is spatially unstable, there being a temporally stable steady flow for which small changes at the inlet or outlet create substantial effects all along the channel. The choice of a sector as the shape of the channel is to permit the exploitation of knowledge of the spatial modes of Jeffery–Hamel flows, although we regard the sector as an example of channels with walls of moderate curvature.

1. Introduction

The flow of a viscous incompressible fluid in a two-dimensional channel poses a classical problem discussed in many textbooks (e.g. Batchelor 1967, §5.6). The problem has a wide range of engineering and environmental applications. It has been studied by use of mathematical, numerical and experimental methods, yet even the early stages of the bifurcations on the route to turbulence are poorly understood.

Asymptotic methods may be used to elucidate the bifurcations and instabilities of the channel flows. One asymptotic approach (cf. Georgiou & Eagles 1985 and earlier papers by Eagles and co-authors) is to assume that the walls of the channel are nearly parallel so that the flow is locally parallel and its instability may be found to the first approximation by solving an Orr–Sommerfeld problem. A similar approach, due to Fraenkel (1962), is to assume that the curvature of the walls of the channel is small so that the flow is locally radial, i.e. a Jeffery–Hamel flow. (Recall that a Jeffery–Hamel flow is a steady two-dimensional radial flow between two inclined rigid planes driven by a line source at the intersection of the planes, and is described exactly by a similarity solution of the Navier–Stokes equations.) We shall mention Jeffery–Hamel flows so often in the paper that it will be useful to call them JH flows.

At this stage it is convenient to define the Reynolds number R in a form suitable for use throughout the paper, namely $R = Q/2\nu$, where Q is the volume flux per unit distance normal to the plane of flow, and ν is the kinematic viscosity of the fluid. Thus we suppose that the flow is driven steadily with flux $Q > 0$. The advantage of this definition is that it does not directly involve a length scale of the channel, and so is suitable for all two-dimensional channel flows driven steadily. There is nothing very special about the choice of the factor $\frac{1}{2}$, but it will simplify some of our arithmetic.

On using the approximation of nearly parallel flow, it is found that instability arises at a large value of R . The mode of instability is a travelling wave, i.e. the principle of exchange of stabilities is invalid; so it may be presumed that there is a Hopf bifurcation with the onset of a time-periodic flow as the Reynolds number increases (although the time-periodic flow may be subcritical and so unstable).

Banks, Drazin & Zaturka (1988) followed Fraenkel's approach and went on to consider the spatial and temporal stability of Jeffery–Hamel flows. The analysis by Banks *et al.* of steady spatial perturbations of a JH flow, developing the pioneering ideas of Dean (1934), suggests that the flow is spatially stable for values of the Reynolds number $R < R_2(\alpha)$, where α is the semi-angle between the plane walls and R_2 is a certain known function. It is similarly stable to symmetric perturbations when $R < R_3(\alpha)$. In practice the flow may be simulated in the laboratory by flow in a channel shaped like a sector with an inlet at an arc of small radius and an outlet at an arc of large radius. Then the analysis suggests that when $R > R_2(\alpha)$ the inlet and outlet conditions affect the whole steady flow, i.e. even if the inlet were at a very small radius and the outlet at a very large radius, there would be significant end effects throughout the domain of flow, and, further, no JH flow would be observed locally at any station. The value $R_2(\alpha)$ of the Reynolds number at the onset of instability is a moderate one (unless α is small), and the mode of instability is a small rotation of the basic flow, the principle of exchange of stabilities being valid; there is a corresponding subcritical pitchfork bifurcation, such that there is an unstable symmetric solution for small $R - R_2(\alpha) > 0$ and a stable symmetric solution and two unstable asymmetric solutions for small $R - R_2(\alpha) < 0$.

The words 'spatial stability' are used so often in this paper that it is appropriate to note that they concern not so much stability, which is usually meant to describe the evolution of perturbations in time, as the behaviour in space of steady flows near to the basic steady flow under consideration. The close relationship of the bifurcation of steady flows to their temporal instability justifies the common usage of the phrase 'spatial stability', even when it strictly concerns only the development of steady flows in space. So spatial stability determines stability indirectly. However, it should not be forgotten that our concentration on steady flows and their spatial stability gives no information about temporal instabilities at Hopf bifurcations, and that such instabilities may be important physically, especially at small values of α for which R_2 is large, and it is known that parallel flows have a subcritical Hopf bifurcation (cf. Drazin & Reid 1981, Chap. 4).

If a channel has walls which are both nearly parallel and of small curvature then we presume that both the Orr–Sommerfeld and Jeffery–Hamel modes of instability may occur. The one which would occur in practice as the Reynolds number is increased very slowly seems to depend upon the details of the configuration of the channel, such as the small angle between the walls and the small curvature.

Cliffe & Greenfield (1982), Sobey & Drazin (1986) and Fearn, Mullin & Cliffe (1990) have found the steady flows in various channels by direct numerical integration of the governing Navier–Stokes equations; Sobey & Drazin also found some time-periodic

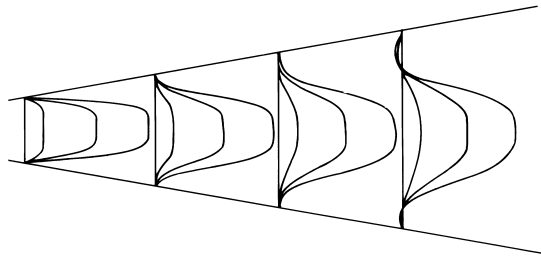


FIGURE 1. Sketch based on Nakayama's experimental results showing hydrogen bubble profiles:
 $R = 300, \alpha = \pi/18$.

flows. In each of the three papers it is found that for a symmetric channel there is a unique stable flow for small values of the Reynolds number R , but that as R increases above a certain critical value, R_c say, the flow becomes unstable and there is a supercritical pitchfork bifurcation such that for small $R - R_c > 0$ there are two stable asymmetric steady flows as well as the unstable symmetric steady flow. The symmetric channels considered in these papers are rather different, yet it is surprising that Sobey & Drazin found R_c to be much smaller than the other authors found it to be; Sobey & Mullin (1992) suggested that Sobey & Drazin's values are inaccurate because of their use of upwind differences. Another surprising result is that the pitchfork bifurcation found in these papers on computational fluid dynamics is supercritical yet the pitchfork bifurcation of JH flows which is associated with their instability and symmetry breaking is subcritical at $R = R_2$ (recall that the JH flow is described by a similarity solution); it follows that there is no JH flow of the computed type to approximate the flow locally in a channel with walls of small curvature when $R > R_c$. So it appears that JH flows are irrelevant to flow in a diverging channel with walls of small curvature if $R > R_c$ or, at least, irrelevant where there is no stable local JH flow. The exact symmetry of the channel is not crucial to these conclusions, although the pitchfork bifurcation is an idealization of an exactly symmetric channel (cf. Sobey & Drazin 1986; Fearn *et al.* 1990). Borgas & Pedley (1990) have also used similarity solutions to find supercritical bifurcations in an indented channel.

Hamadiche, Scott & Jeandel (1994) have recently investigated the temporal stability of some of the symmetric JH flows. They posed the linearized eigenvalue problem on a finite sector and proceeded to determine the critical value of the Reynolds number corresponding to marginal stability for various values of the semi-angle α . They found that 'loss of stability is supercritical' (when α is not very small) although their marginal curves 'are in surprisingly good agreement' with the solutions of Sobey & Drazin (1986, §3) of the model stability problem of Hooper, Duffy & Moffatt (1982).

There have been many laboratory experiments on flows in diverging channels at various values of the Reynolds number R , but few (e.g. Sobey & Drazin 1986; Fearn *et al.* 1990) have been carefully related to theoretical results. Nakayama (1988, figure 105) has published a single photograph of flow along a diverging channel with plane walls at a semi-angle of $\alpha = 10^\circ$, i.e. $\alpha = \pi/18$ radians, at $R = 300$. We have prepared a sketch of Nakayama's experimental results from his figure 105 and present them in figure 1. This is a model of a diffuser, as if designed to represent a JH flow: yet the flow shown has an asymmetric velocity profile with reverse flow near each wall, and no such JH flow exists. Again, we are drawn to the conclusion that, even if of all the local JH flows which exist none is stable, the flow in a channel may be steady and stable yet of a form different from a JH solution.

The aim of this paper is to clarify some of these difficulties by use of computational fluid dynamics. By judicious choice of problems and careful numerical methods we have tried to bridge the gap between the mathematical results and previous numerical and experimental results, and resolve some of the paradoxes we have just described. In particular, we confirm the conjecture of Banks *et al.* (1988) that of the two families of eigenvalues known analytically for $R = 0$, one is associated with the growth or decay for increasing r and the other for decreasing r .

2. Flow in a sector

2.1. Formulation of problem

On the basis of the preceding discussion, we recognize that the problem of two-dimensional flow in a channel, whose shape is a sector with an inlet at an arc and an outlet at another arc, is fundamental to understanding flows in diverging channels with small curvature. Banks *et al.* (1988) posed this problem mathematically, but Bühler & Krückels (1990) initiated its numerical solution; however, their calculations were few, made in short channels, and made for flows for which an unstable JH velocity is imposed at the outlet although a stable JH flow exists at the values of R, α used. Accordingly, we shall now formulate the problem, as illustrated in figure 2, and proceed to solve it numerically. Take plane polar coordinates (r, θ) and corresponding velocity components of the fluid as u, v respectively. We suppose that a steady flow is driven by a given volume flux Q between the rigid impermeable walls with equations $\theta = \pm\alpha$, and that the inlet arc has equation $r = r_1$ and the outlet arc $r = r_2 > r_1$. It is convenient to use a streamfunction ψ such that $u = \partial\psi/r\partial\theta$ and $v = -\partial\psi/\partial r$. Then the vorticity may be written as

$$\zeta = -\nabla^2\psi \tag{2.1}$$

and the Navier–Stokes equations reduce to the vorticity equation,

$$\frac{1}{r} \frac{\partial(\zeta, \psi)}{\partial(r, \theta)} = \nu \nabla^2 \zeta, \tag{2.2}$$

where the Laplacian in cylindrical polar coordinates is $\nabla^2 = \partial^2/\partial r^2 + \partial/r\partial r + \partial^2/r^2\partial\theta^2$. Also the boundary conditions are

$$\psi = \pm\frac{1}{2}Q, \quad \frac{\partial\psi}{\partial\theta} = 0 \quad \text{at } \theta = \pm\alpha \tag{2.3}$$

respectively on the sidewalls,

$$\psi = f_1(\theta), \quad \frac{\partial\psi}{\partial r} = g_1(\theta) \quad \text{at } r = r_1 \tag{2.4}$$

at the inlet, and

$$\psi = f_2(\theta), \quad \frac{\partial\psi}{\partial r} = g_2(\theta) \quad \text{at } r = r_2 \tag{2.5}$$

at the outlet, where the choice of $f_1(\theta), g_1(\theta), f_2(\theta), g_2(\theta)$ (such that $f_1(\pm\alpha) = f_2(\pm\alpha) = \pm\frac{1}{2}Q, f'_1(\pm\alpha) = f'_2(\pm\alpha) = g_1(\pm\alpha) = g_2(\pm\alpha) = 0$) specifies the inlet and outlet velocities consistently with the given flux. We also consider in §3 replacing the condition on $\partial\psi/\partial r$ at $r = r_1, r_2$ by a condition on ζ , and in §4 discuss the relationship of the inlet and outlet conditions to laboratory experiments.

It is, of course, convenient to use dimensionless variables. So write $r = r_1 r', r_2 = r_1 r'_2, \psi = \frac{1}{2}Q\psi', \zeta = Q\zeta'/2r_1^2$, and rescale the inlet and outlet conditions. Then drop

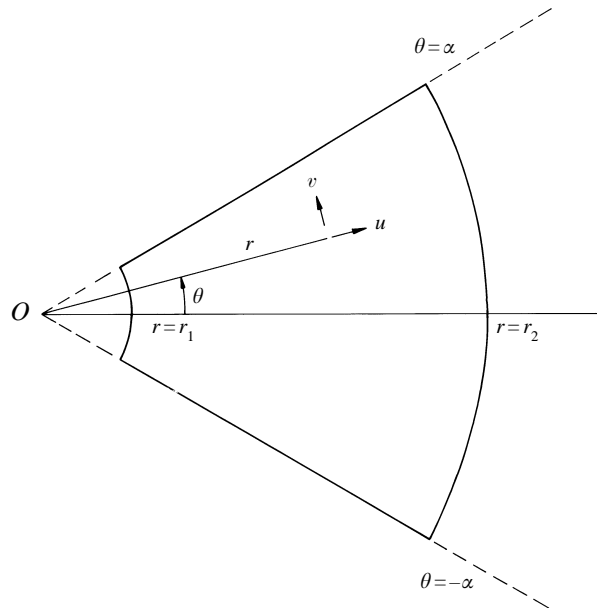


FIGURE 2. Sketch of the configuration of flow in a sector.

the primes so that (2.1) remains unchanged and the problem reduces to

$$\frac{1}{r} \frac{\partial(\zeta, \psi)}{\partial(r, \theta)} = R^{-1} \nabla^2 \zeta, \tag{2.6}$$

$$\psi = \pm 1, \quad \frac{\partial \psi}{\partial \theta} = 0 \quad \text{at } \theta = \pm \alpha, \tag{2.7}$$

$$\psi = f_1(\theta), \quad \frac{\partial \psi}{\partial r} = g_1(\theta) \quad \text{at } r = 1, \quad \psi = f_2(\theta), \quad \frac{\partial \psi}{\partial r} = g_2(\theta) \quad \text{at } r = r_2, \tag{2.8}$$

where the Reynolds number is defined as

$$R = Q/2\nu. \tag{2.9}$$

2.2. Jeffery–Hamel flows

Before describing our numerical method for solving (2.1), (2.6), (2.7) and (2.8), we recall briefly the results of the Jeffery–Hamel similarity solution. For this, boundary conditions (2.8) are ignored and a steady solution is sought in the form

$$\psi = G(y, \alpha, R), \tag{2.10}$$

where $y = \theta/\alpha$. Then problem (2.1), (2.6), (2.7) reduces to

$$G^{iv} + 4\alpha^2 G'' + 2\alpha R G' G'' = 0, \tag{2.11}$$

$$G = \pm 1, \quad G' = 0 \quad \text{at } y = \pm 1, \tag{2.12}$$

where a prime denotes differentiation with respect to y .

Much is known about these exact solutions, $G(y, \alpha, R)$, of the Navier–Stokes equations and a summary of the results is given by the diagram in figure 3: fuller details are given by Fraenkel (1962), but they are too complicated to state here apart from

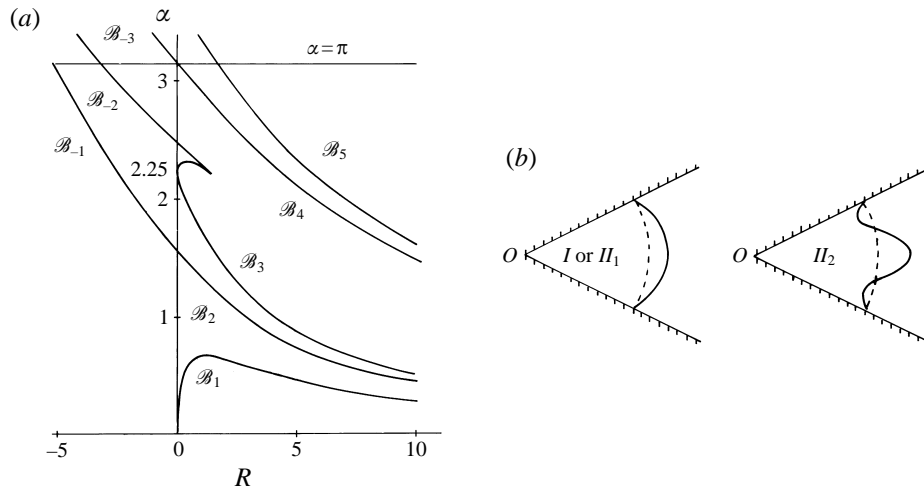


FIGURE 3. (a) Boundaries \mathcal{B}_n for some types of Jeffery–Hamel solutions in the (R, α) -plane (after Banks *et al.* 1988, figure 3). Solutions of type *I* arise for values of (R, α) lying between the R -axis and curve \mathcal{B}_1 , of type II_n between the curves \mathcal{B}_{n-1} and \mathcal{B}_n , and symmetric solutions of type III_n with net inflow arise for $R < 0$. (b) Sketches of velocity profiles of flows of types *I*, II_1 , and II_2 .

the chief points relevant to the present work. It will be convenient to note that the pressure can be written as

$$p = \frac{2(G' + C)}{\alpha R r^2}, \quad (2.13)$$

where C is a constant, on absorbing any additional constant in the initial non-dimensionalization. There is an infinity of solutions, both symmetric and antisymmetric, for any given pair of values of R, α . Fraenkel denoted the types of the solutions by the letters *I*, II_n , III_n , IV_n , V_n , where n is a ‘counter’ for the number of maxima and minima of the velocity profiles belonging to each type. The regions of the (R, α) -plane where a few of the solutions occur is indicated in figure 3(a), and the velocity profiles of the most relevant solutions *I*, II_1 , II_2 are sketched in figure 3(b).

Various perturbations of the JH solutions have been studied, but here we shall study the spatial development of such steady flows and their steady perturbations after Banks *et al.* (1988) and Goldshtik, Hussain & Shtern (1991); on writing

$$\psi(r, \theta, \alpha, R) = G(y, \alpha, R) + r^\lambda \hat{\psi}(y, \alpha, R), \quad (2.14)$$

substituting into (2.1), (2.6) and (2.7), and linearizing, an eigenproblem is derived with value $\lambda = \lambda(\alpha, R)$. Little is known of the properties of $\lambda(\alpha, R)$ for $R \neq 0$ but $\lambda(\alpha, 0)$ is known analytically: there are two families. Each family can be divided into two infinite subfamilies, with one subfamily of antisymmetric modes and another of symmetric modes, say A_+^a, A_+^s respectively with $\text{Re}(\lambda) > 1$ and A_-^a, A_-^s with $\text{Re}(\lambda) < 1$. We have conjectured that the subfamilies A_+^a, A_+^s represent the spatial growth (or decay) of steady disturbances as r decreases, while the subfamilies A_-^a, A_-^s represent the growth of disturbances as r increases. We also conjecture that the same subfamilies occur when $R \neq 0$ although their quantitative details differ from those when $R = 0$.

Finally we note that the leading or most ‘dangerous’ mode of the subfamilies A_+^a, A_+^s , dangerous only in the sense that it grows most rapidly as r decreases, is antisymmetric, i.e. of all the modes belonging to A_+^a, A_+^s the one with the minimum

value of $\text{Re}(\lambda)$ belongs to A_+^a . Similarly, the mode of the subfamilies A_+^a, A_-^s with maximum value of $\text{Re}(\lambda)$ is antisymmetric. So we anticipate that flow in a half-sector $0 \leq y \leq 1$ (with symmetry boundary conditions on the symmetry plane $y = 0$) may be spatially stable whereas flow in a full sector may be unstable for the same value of R .

3. Numerical method for steady flow

Next we shall briefly describe the numerical formulation which we used to solve equations (2.1), (2.6), reverting to dimensional form.

The sectorial region $r_1 \leq r \leq r_2, -\alpha \leq \theta \leq \alpha$ of figure 2 is divided into the polar grid

$$r = r_1 + jh_1, \text{ for } j = 0, 1, \dots, J; \theta = -\alpha + kh_2 \text{ for } k = 0, 1, \dots, K, \quad (3.1)$$

where $h_1 = (r_2 - r_1)/J, h_2 = 2\alpha/K$. At any node (r, θ) of this grid, the spatial derivatives which appear in (2.1) and (2.6) are approximated by the usual central-difference formulae. This gives the respective approximations to (2.1), (2.6) at this point as

$$(1 + h_1/2r)\psi(r + h_1, \theta) + (1 - h_1/2r)\psi(r - h_1, \theta) + (\gamma^2/r^2)[\psi(r, \theta + h_2) + \psi(r, \theta - h_2)] - 2(1 + \gamma^2/r^2)\psi(r, \theta) + h_1^2\zeta(r, \theta) = 0, \quad (3.2)$$

$$\begin{aligned} & [1 + h_1/2r - (\gamma R/4r)\{\psi(r, \theta + h_2) - \psi(r, \theta - h_2)\}]\zeta(r + h_1, \theta) \\ & + [1 - h_1/2r + (\gamma R/4r)\{\psi(r, \theta + h_2) - \psi(r, \theta - h_2)\}]\zeta(r - h_1, \theta) \\ & + [\gamma^2/r^2 + (\gamma R/4r)\{\psi(r + h_1, \theta) - \psi(r - h_1, \theta)\}]\zeta(r, \theta + h_2) \\ & + [\gamma^2/r^2 - (\gamma R/4r)\{\psi(r + h_1, \theta) - \psi(r - h_1, \theta)\}]\zeta(r, \theta - h_2) \\ & - 2(1 + \gamma^2/r^2)\zeta(r, \theta) = 0, \end{aligned} \quad (3.3)$$

where $\gamma = h_1/h_2$.

Equations (3.2), (3.3) form two sets of equations which are obtained by setting (r, θ) equal to the coordinates of each grid point in the region, and these must be solved numerically. The given boundary conditions for ψ are of Dirichlet type for (3.2), but it is necessary to calculate boundary values for ζ by using all the conditions in (2.7), (2.8). Both the approximations (3.2), (3.3) are h^2 -accurate, so it is desirable to obtain h^2 -accurate approximations to the boundary values of ζ . We have done this by following the procedure of Woods (1954) in which ψ is expanded as a Taylor series in the appropriate variable normal to the boundary concerned. The corresponding normal gradient condition is used in this expansion, and higher derivatives are determined from equation (2.1); this leads to an approximation to the boundary value of ζ in terms of internal values of ψ, ζ at the nearest grid point along the appropriate normal direction.

The procedure is illustrated for the case of the boundary conditions at $r = r_1, r_2$. If we take $r = r_1$ as typical, we obtain

$$\psi(r_1 + h_1, \theta) = f_1(\theta) + h_1 g_1(\theta) + \frac{1}{2}h_1^2 \left[\frac{\partial^2 \psi}{\partial r^2} \right]_1 + \frac{1}{6}h_1^3 \left[\frac{\partial^3 \psi}{\partial r^3} \right]_1 + O(h_1^4) \quad (3.4)$$

as $h_1 \rightarrow 0$, where we denote the value of a function at $r = r_1$ by the subscript 1. The second derivative $\partial^2 \psi / \partial r^2$ can be expressed in terms of $\zeta, \partial \psi / \partial r, \partial^2 \psi / \partial \theta^2$ at $r = r_1$ from (2.1) and the third derivative can be obtained by differentiation of (2.1). The

third derivative involves $\partial\zeta/\partial r$ and if we express this at $r = r_1$ in the form

$$\frac{\partial\zeta}{\partial r} = (\zeta_I - \zeta_1)/h_1 + O(h_1), \quad (3.5)$$

where I denotes the grid point next to $r = r_1$ along the normal, and neglect the error terms in (3.4), (3.5), we finally obtain the approximation

$$(1 - h_1/2r_1)\zeta_1(\theta) = -(3/h_1^2)[\psi_I(\theta) - f_1(\theta) - h_1g_1(\theta)] - \frac{1}{2}\zeta_I(\theta) \\ - (3/2r_1)(1 - 2h_1/3r_1)g_1(\theta) - (3/2r_1^2)(1 - h_1/r_1)f_1''(\theta) - (h_1/2r_1^2)g_1''(\theta), \quad (3.6)$$

which is h^2 -accurate. This holds for all grid points on $r = r_1$, and there is a similar formula for $\zeta_2(\theta)$ at grid points on $r = r_2$. This is obtained from (3.6) simply by changing h_1 to $-h_1$ and modifying the subscripts of $\psi_1, \zeta_1, f_1, g_1, r_1$ to 2; the subscript I still refers to the grid point next to r_2 along the normal direction on the fluid side.

For the conditions on $\theta = \pm\alpha$ we used exactly the same method of expanding along the inward normal, and find

$$\zeta_{\pm\alpha}(r) = \frac{3}{h_1^2 r^2} [\psi_{\pm\alpha}(r) - \psi_I(r)] - \frac{1}{2}\zeta_I(r) \quad (3.7)$$

for all grid points on $\theta = \pm\alpha$, where again I denotes the internal grid point nearest to the boundary; equation (3.7) holds on both $\theta = \pm\alpha$, and r refers to the grid point under consideration. This completes the numerical formulation of the problem. We have to solve the finite-difference equations (3.2), (3.3) for all internal grid points by some form of matrix inversion, and at the same time satisfy all the boundary conditions, which means that equations (3.6) on $r = r_1, r_2$ and (3.7) on $\theta = \pm\alpha$ must also be satisfied.

An iterative method was used. An approximate solution of equations (3.2), (3.3) was obtained and then used to calculate the right-hand sides of (3.6), (3.7) in order to estimate $\zeta_1(\theta), \zeta_2(\theta), \zeta_{\pm\alpha}(r)$. Successive over-relaxation was used to solve equations (3.2), (3.3), and relaxation is also necessary to calculate the boundary values of ζ from (3.6), (3.7). For both equations under-relaxation is necessary since the calculations are very sensitive owing to the large factors multiplying some of the terms on the right-hand sides when h_1, h_2 are small. Thus if $\zeta^{(c)}$ denotes the calculated boundary value of ζ from equation (3.6) or (3.7) at any iteration $\zeta^{(k)}$ of the procedure, then the next approximation to the boundary value was taken as

$$\zeta^{(k+1)} = (1 - \omega)\zeta^{(k)} + \omega\zeta^{(c)}, \quad (3.8)$$

where ω is a relaxation parameter. It is necessary to take $\omega \ll 1$ in order that the iterative procedure converges. The same equation (3.8) defines the over-relaxation procedure which was applied to ζ at each grid point in the numerical solution of (3.3), but here we can take $\omega \geq 1$, in general. A similar equation was used for ψ during solution of (3.2); here we can again take $\omega \geq 1$ though not necessarily the same as that applicable to the determination of ζ from (3.3). In all cases the choice of ω depends upon the Reynolds number and also, to some extent, upon the grid sizes.

The whole iterative procedure was in fact carried out by performing one operation through the complete set of equations (3.3) followed by a complete iteration through (3.2). Then, boundary values were calculated according to equations (3.6), (3.7) by using (3.8). This whole procedure was repeated until numerical convergence according to the criterion

$$\sum_n |\zeta_n^{(k+1)} - \zeta_n^{(k)}| < \epsilon_1, \quad \sum_n |\psi_n^{(k+1)} - \psi_n^{(k)}| < \epsilon_2, \quad (3.9)$$

where ϵ_1, ϵ_2 are assigned small parameters and n is the total number of grid points. The parameters ϵ_1, ϵ_2 depend upon the grid sizes. In the numerous solutions obtained, some of which are reported below, it was customary to obtain more accurate solutions, for given R, α and boundary conditions, by successively halving the grid sizes in both directions. However, for consistency in applying the convergence criteria in (3.9), the parameters ϵ_1, ϵ_2 should be quadrupled on each occasion that the grid is halved. Furthermore, some degree of care is needed to ensure that numerical convergence has taken place when the number of grid points is large. Thus, in the end, a visual inspection of the boundary values of vorticity was also made after a fixed number of iterations following the satisfaction of the tests (3.9), in order to ensure that no significant change took place.

4. Numerical results

Using a scheme of the form described in §3, we solved the steady problem (2.1), (2.6), (2.7) and the set of boundary conditions (2.8). Also, it is convenient, in view of the Jeffery–Hamel similarity solution governed by (2.11) and (2.12), to make the change of variable $\zeta = \phi r^{-2}$ in (2.6) which makes ϕ independent of r in the similarity solution and thus more readily approximated by finite differences. This transformation merely adds terms

$$R^{-1} \left\{ -\frac{4}{r} \frac{\partial \phi}{\partial r} + \frac{2}{r^2} \left(2 + R \frac{\partial \psi}{\partial \theta} \right) \phi \right\}$$

to the right-hand side of (2.6), when expressed in terms of ϕ . The changes which need to be made in the various equations of §3 and in the boundary conditions are fairly routine and are not given here.

A number of trial solutions were first carried out to test the numerical method, e.g. with the boundary conditions (2.8) given by

$$f_1(\theta) = 3\theta(1 - \theta^2/3\alpha^2)/2\alpha, \quad f_2(\theta) = \theta/\alpha, \quad g_1(\theta) = g_2(\theta) = 0, \quad (4.1)$$

and, in dimensionless variables, with $r_1 = 1, r_2 = 7, \alpha = 1$. (These values of r_1, r_2 were used thereafter except where stated otherwise. They were chosen somewhat arbitrarily, but give an aspect ratio r_2/r_1 which is large enough to observe whether some flows settle down to JH flows or not, small enough to prevent the need for very expensive calculations, and close enough to the value for the channel in the experiment of Nakayama (1988, figure 105).) Several Reynolds numbers were considered and three grids were employed in each case, namely $h_1 = 0.25, h_2 = 0.05$ followed by the two grids obtained by successively halving each grid length. Use of h^2 -extrapolation enabled us to check the accuracy. For the lower Reynolds numbers it was possible to use relaxation parameters ω of 1.4 or 1.5 for ζ and ψ with very rapid numerical convergence, but these had to be gradually reduced as R was increased. The relaxation factors appropriate to (3.6) and (3.7) were generally less than 0.5, reducing to 0.05 for higher values of R . Care is necessary to ensure complete numerical convergence when ω is as low as 0.05. Finally, the numerical results of these tests indicated good accuracy with a very clear approach to limit solutions as $h_1, h_2 \rightarrow 0$.

The method outlined in §3 was also modified to deal with boundary conditions of the form

$$\psi = f_1(\theta), \quad \zeta = z_1(\theta) \text{ at } r = r_1, \quad \psi = f_2(\theta), \quad \zeta = z_2(\theta) \text{ at } r = r_2. \quad (4.2)$$

Here too, in order to check the computer coding and to estimate the numerical errors,

we chose values of α, R for $R_2 > R \geq 0$, and assigned to $f_i(\theta), z_i(\theta), i = 1, 2$, the forms corresponding to the JH solutions. It was then found that the calculated solutions ψ were approximately independent of r . Various grids were used and the results found to be consistent: with h^2 -extrapolation we obtained agreement to six decimal places with solutions of the ordinary differential system (2.11), (2.12) found by using a Runge–Kutta–Merson method.

It will help, while interpreting the results below, to recall that a basic symmetric flow in the full sector $-\alpha \leq \theta \leq \alpha$ may be (i) stable to all small perturbations, (ii) unstable, yet stable to all small symmetric perturbations, or (iii) unstable to at least one antisymmetric and one symmetric mode of perturbation. To highlight this, we have made some numerical experiments in the half sector $0 \leq \theta \leq \alpha$ with boundary conditions ($\psi = \partial^2\psi/\partial\theta^2 = 0$) at $\theta = 0$ satisfied by all symmetric solutions over the full sector. By reflection in $\theta = 0$, the solution in the half sector gives a symmetric solution in the full sector. The theory of linear spatial stability suggests that in case (i) $R < R_2(\alpha)$ and flows in both the full and half sectors are stable; in case (ii) $R_2(\alpha) < R < R_3(\alpha)$ and the flows in the full sector are unstable but flows in the half sector are stable; and in case (iii) $R_3(\alpha) < R$ and all JH flows in the full and half sectors are unstable, and there exists neither a symmetric nor an asymmetric JH flow with a single maximum of the velocity.

With $R = 0$ we verified the predictions of perturbation theory which are described briefly at the end of §2. For $\alpha = 1$ we chose $f_1(\theta) = G(y, 1, 0), z_1(\theta) = -r_1^{-2}G''(y, 1, 0)$ and $f_2(\theta) = G(y, 1, 0) + r_2^{l_1}\hat{\psi}(y, 1, 0), z_2(\theta) = -r_2^{-2}G''(y, 1, 0) - r_2^{l_1-2}(\hat{\psi}'' + l_1^2\hat{\psi})$, where $l_1 (= 3.1841798 + 0.6890455i$ for $\alpha = 1$), $\hat{\psi}$, is the leading mode belonging to A_+^a . (Note that $\alpha_2(0) = \frac{1}{2}\pi > 1 = \alpha$.) Since $R = 0$ the linearization gives the exact solution of the perturbed problem and the normalization of $\hat{\psi}$ is not important. In this way we verified the spatial decay of the disturbance at r_2 as r decreases to r_1 . We repeated the calculation with the disturbance imposed at $r = r_1$, but with the forms $r_1^{l_1-1}\hat{\psi}$ and $-r_1^{(l_1-2)}(\hat{\psi}'' + l_1^2\hat{\psi})$ added to $f_1(\theta)$ and $z_1(\theta)$ respectively. The mode here with $l_{-1} (= -1.1841798 + 0.6890455i$ for $\alpha = 1$) is the leading mode for r increasing and belongs to A_-^a . We again found that this disturbance decays as r increases to r_2 . We remark that some of these solutions are, of course, asymmetric. It is possible to impose boundary conditions at both r_1 and r_2 by reference to (2.14), with $\lambda = l_1$ or l_{-1} depending on whether the disturbance decays as r decreases to r_1 or increases to r_2 respectively. This was done and our numerical results agreed well with the exact result (2.14). We have not displayed any results concerning the pressure, but merely note from equation (2.13) that the Stokes pressure (i.e. Rp in the limit as $R \rightarrow 0$) is inversely proportional to the square of the distance downstream.

We conclude plausibly that the numerical method and the coding of the problem are satisfactory. It should be noted, however, that we could not evaluate the eigenvalues from the numerical solutions of the partial differential problem. We presume that this is because several modes are superposed in the numerical solutions, the modes decay too slowly (their decay being algebraic) and the sector is not long enough (with ratio r_2/r_1 only 7) for the leading mode to dominate the others anywhere.

Before describing our results for $R \neq 0$, we describe those for $R = 0$ and $\alpha_2 < \alpha < \alpha_3$, where $R_2(\alpha_2) = 0, R_3(\alpha_3) = 0$; in fact $\alpha_2 = \frac{1}{2}\pi, \alpha_3 \approx 2.246$ when $R = 0$. The value $\alpha = 1.7$ was chosen as ‘typical’ to ensure in this way that the JH flow (of type II_2) in the full sector is spatially unstable to the l_1 and l_{-1} antisymmetric modes, although the JH flow in a half sector is spatially stable to all modes (2.14).

For boundary conditions, we first imposed the appropriate JH solution (of type

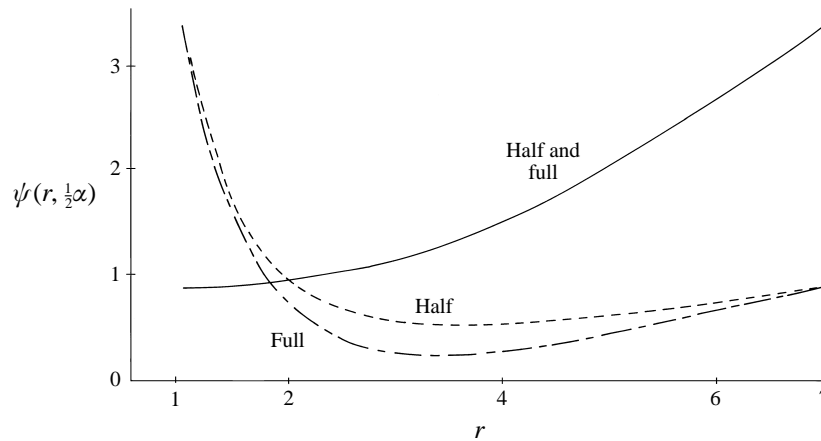


FIGURE 4. Values of $\psi(r, \frac{1}{2}\alpha)$ against r for $R = 0, \alpha = 1.7$ for flows in the full and half sectors: solid curve for the perturbation imposed at $r = r_2$ (the results for the full and half sectors are indistinguishable); broken curve for the half sector with the perturbation imposed at $r = r_1$; chained curve for the full sector with the perturbation imposed at $r = r_1$.

I, II_1 or II_2) at both $r = r_1$ and r_2 ; the results for both full and half sectors were the same and the solutions were approximately independent of r . Even though the flow is predicted to be spatially unstable in the full sector, the calculation failed to reveal this instability. So we next investigated the effect of perturbations at $r = r_1$ and r_2 in turn: we added $(\alpha^2 - \theta^2)^2\theta^4$ (i.e. an antisymmetric disturbance) to the basic JH streamfunction. We found that, irrespective of whether the problem is posed in the half or full sector, when the disturbance is imposed at $r = r_2$ the approach to the JH solution at $r = r_1$ is monotonic, whereas if the disturbance is imposed at $r = r_1$ there is an overshoot in the approach to the JH solution at $r = r_2$. Further, when the disturbance is imposed at $r = r_2$ there is very little difference between the full- and half-sector results, but there is a significant difference when the disturbance is imposed at $r = r_1$. We presume that this difference is due to the relative size of the two leading antisymmetric eigenvalues from A_+^a and A_-^a ($= 1.85891$ and 0.14109 respectively) and the shortness of the channel ($r_2/r_1 = 7$). The plots of $\psi(r, \frac{1}{2}\alpha)$ in figure 4 illustrate these properties; note that the results for the half and full sectors clearly differ when the JH flow is perturbed at $r = r_1$. We anticipate that the overshoot in the full sector becomes greater as the radius ratio is increased: we confirm this later for some other values of α and R when the ratio is increased.

We next present results for $R > 0$. We chose $\alpha = 1$ and sought solutions in both the full and half sectors with $2.9 = R_2(1) < R < R_3(1) = 4.4$: we chose $R = 3.5$ as 'typical'. It will be noted that, as for $R = 0, \alpha = 1.7$, the JH flow in a full sector is spatially unstable while that in a half-sector is stable to the modes (2.14). We started the calculations by imposing the JH solution at $r = r_1$ and r_2 in both the full- and half-sector configurations, and both sets of results agree with the known JH solution to about 5 significant figures: the flow predicted is again independent of r . This is the same as when $R = 0, \alpha = 1.7$. Indeed, even when the streamfunction at $r = r_1, r_2$ is perturbed by the addition of $(\alpha^2 - \theta^2)^2\theta^4$, the results are still similar to those for $R = 0, \alpha = 1.7$. However, we proceeded further in this case by increasing the radius ratio r_2/r_1 of the sector from 7 to 13 and finally to 25. With the perturbation imposed at $r = r_2$, the results for the full sector differed very little (about 0.02%): note that

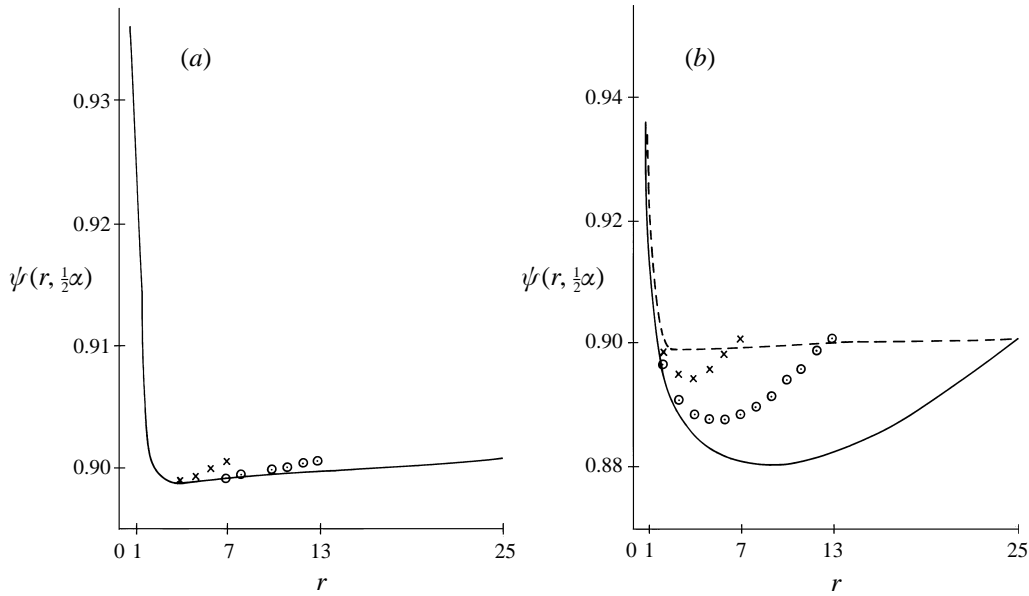


FIGURE 5. Values of $\psi(r, \frac{1}{2}\alpha)$ against r for $R = 3.5, \alpha = 1$ and various ratios r_2/r_1 . (For unperturbed JH flow the curve would be the horizontal line $\psi(r, \frac{1}{2}\alpha) = 0.89857$.) (a) The flow in the half sector, with the perturbation imposed at $r = r_1$. The solid curve denotes the results for $r_2/r_1 = 25$, \odot for $r_2/r_1 = 13$, \times for $r_2/r_1 = 7$. (b) The flow in the full sector, with the perturbation imposed at $r = r_1$. The solid curve denotes the results for $r_2/r_1 = 25$, \odot for $r_2/r_1 = 13$, \times for $r_2/r_1 = 7$. The analogous results for the half sector with r_2/r_1 , shown by a broken curve are repeated for comparison.

for this comparison it was necessary to re-scale the interval $r_1 < r < r_2$. Further note that, as reported for $R = 0, \alpha = 1.7$, the difference between the full- and half-sector solutions was small (typically about 0.1%) when the perturbation was imposed at $r = r_2$. With the perturbation imposed at $r = r_1$, however, the difference between the full- and half-sector solutions increases as the radius ratio is increased: for the half sector, increasing the ratio changes the results very little, but for the full sector it changes them substantially. The plots of $\psi(r, \frac{1}{2}\alpha)$ in figure 5 illustrate these properties, showing the effect of lengthening both the half and full sectors. Note that lengthening the full sector increases the overshoot. All this confirms that the basic JH flow in the half sector is stable but that in the full sector is not.

Consider next values of α, R at which there is no JH solution with uniformly outward flow, i.e. with radial velocity $u \geq 0$ for all θ . We chose $\alpha = 1$ again, with $R = 7.5 (> R_3(1) = 4.4)$, for our calculations. Because there is no uniformly outward JH solution on which to base the boundary conditions, we imposed at $r = r_1, r_2$ the Stokes solution for $\alpha = 1, R = 0$, namely

$$G(y, 1, 0) = \frac{\sin 2y - 2y \cos 2}{\sin 2 - 2 \cos 2},$$

together with the vorticity associated with this streamfunction.

We found that the results for the full and half sectors are the same: the flow in the full sector is symmetric and coincides with the flow found for the half sector. However, adding $(1 - \theta^2)^2 \theta^4$ to the streamfunction at the inlet $r = r_1$ in order to perturb the flow asymmetrically, we found that the flow in the full sector is changed much more than the flow in the half sector. Similarly, adding the same perturbation

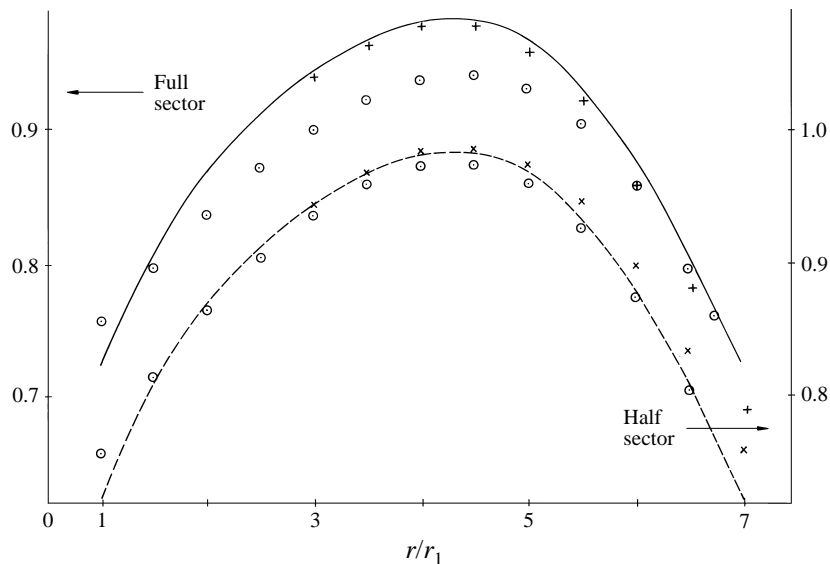


FIGURE 6. Values of $\psi(r, \frac{1}{2}\alpha)$ against r for $R = 7.5, \alpha = 1$. The values for flow in the full sector with no perturbation are shown by a full curve, those for flow in the half sector, also with no perturbation, by a broken curve. The corresponding cases with the perturbation imposed at $r = r_1$ are shown by \odot , and with the perturbation imposed at $r = r_2$ are shown for the full sector by $+$ and for the half sector by \times . Note the displaced scales for the two distinct cases.

at the outlet, we found that the flow in the full sector is changed more than the flow in the half sector, but the difference is much greater when the inlet condition is modified. The plots of $\psi(r, \frac{1}{2}\alpha)$ in figure 6 illustrate these properties. Note that, for a flow in either the half or the full sector, the results when the perturbation is imposed at $r = r_1$ cross those of the unperturbed flow. All these results suggest that the flow in the full sector is unstable but the flow in the half sector is stable, although more calculations with larger radius ratios are needed to substantiate this suggestion. Also we presume that the eigenvalue belonging to the leading mode in A_+^a has a greater real part than that of the eigenvalue belonging to the leading mode in A_-^a , although both eigenvalues are unknown (we assume that, even though there is no JH flow of physically acceptable form, there are the usual two families of eigensolutions).

For both a comparison of theory and experiment and an example of flow in the full sector with $R \gg R_3(\alpha)$, we sought to simulate the experiment of Nakayama (1988, figure 105). He drove a flow through a channel with $\alpha = \pi/18, R = 300$; we have been unable to ascertain the inlet and outlet conditions, but estimate that the aspect ratio $r_2/r_1 \approx 5$. It appears that his flow was very smooth and steady. Note that the hydrogen-bubble profiles in his photograph are not quite the same as velocity profiles at given radii. Also the observed asymmetric flow (see our figure 1) with one maximum and two minima of the velocity does not correspond to any JH flow; it is plausibly an asymmetric steady flow following a supercritical pitchfork bifurcation at a lower value of the Reynolds number. We have obtained many results for flow in both the full and the half sectors with $\alpha = \pi/18, r_2/r_1 = 7$ and values of R increasing from 5. In the absence of any JH flow for $R > R_3$, we chose as boundary conditions $\psi(r, \theta) = G(y, \alpha, 0)$ for $-\alpha \leq \theta \leq \alpha$ at $r = r_1, r_2$, where G is the Stokes solution together with the associated conditions for the vorticity, and then, in separate calculations,

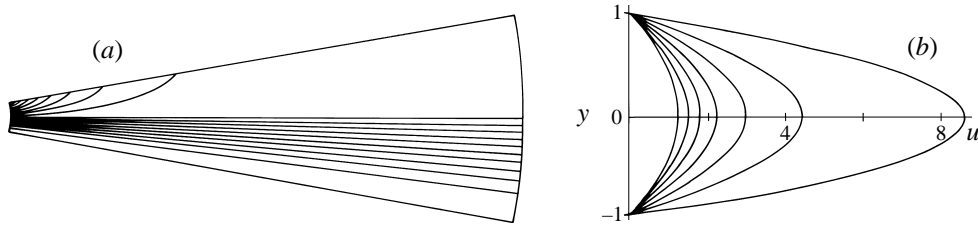


FIGURE 7. Results for $R = 5, \alpha = \pi/18$. (a) Streamlines and vorticity contours. The streamlines, for $\psi = -n/10, n = 0, 1, 2, \dots, 10$, are shown in the lower-half sector and vorticity contours in the upper. (b) Velocity profiles (u versus y) at $r = 1, 2, 3, 4, 5, 6, 7$. (They can be identified by noting that the value of u on the centreline decreases with increasing r .) Note that those profiles corresponding to $r = 1, 7$ are imposed as boundary conditions.

added the perturbations $(1 - (\theta/\alpha)^2)^2(\theta/\alpha)^4$ at $r = r_1$ or r_2 . Next we describe our results with the aid of graphs.

When $R = 5$ the results for the half and full sectors are indistinguishable. They are, moreover, indistinguishable whether the perturbation is imposed at $r = r_1$ or r_2 ; so figure 7(a) shows the streamlines in the lower-half sector and the contours of constant vorticity in the upper-half sector of the symmetric flow. Note that the streamlines are fairly straight and the vorticity is roughly constant in a large area of the sector. Also the velocity profiles at $r = 1, 2, 3, 4, 5, 6, 7$ are shown in figure 7(b) (but remember that the profiles at $r = 1, 7$ are given directly by the boundary conditions). Note that u is approximately inversely proportional to r (as expected because $R < R_2(\pi/18) = 28.68, R_3(\pi/18) = 31.03$). We have found the variation of pressure with r along $\theta = 0, -\alpha/4, -\alpha/2, -3\alpha/4, -\alpha$, and we show the results in figure 8(a). It will be noted that we have plotted $p(r, \theta) - p(1, \theta)$ on each ray so that the pressure drop is clearly evident although the variation is not of inverse-square form.

Similar patterns were found for $R = 10, 25$. However, at $R = 25$ the vorticity contours are appreciably different, as demonstrated in figure 9, which shows the vorticity contours for the flow in the full sector with the perturbation imposed at the inlet $r = r_1$ (detailed investigation of the streamlines near the inlet, shown in figure 10(a), reveals the effect of the perturbation). Note that the flow is nearly symmetric. The velocity profiles at $r = 1, 2, 3, 4, 5, 6, 7$ are shown in figure 10(b) (again the effect of the perturbation is revealed by the figure). Further, the pressure varies with r differently in that it increases for some values of θ . This is clearly shown in figure 8(b) where we display the pressure variation versus r for $\theta = 0, -\alpha/4, -\alpha/2, -3\alpha/4, -\alpha$.

When $R = 50$, the flow in the full sector is again nearly symmetric, but the symmetry can be strikingly broken when a small perturbation is imposed: there may be an eddy with reversed flow near one of the walls. Figure 11 shows the streamlines when a perturbation is imposed at $r = r_2$ and figure 12(a) when it is at $r = r_1$. The occurrence of a closed streamline implies that there is separation and reattachment on the lower wall. Of course, taking the mirror image of the perturbation in the centreline would result in the eddy being near the other wall. The effects of the perturbation at $r = r_2$ are significant only locally. The asymmetry of the streamlines in figure 12(a) can also be seen in a plot of the vortex contours (not shown here). The velocity profiles are shown in figure 12(b). When the flow is symmetric and when the perturbation is imposed at $r = r_2$, the pressure variations along the channel in both cases are similar to that shown in figure 8(b), with any asymmetry confined to the immediate vicinity of $r = r_2$. However when the perturbation is imposed at $r = r_1$ the results do

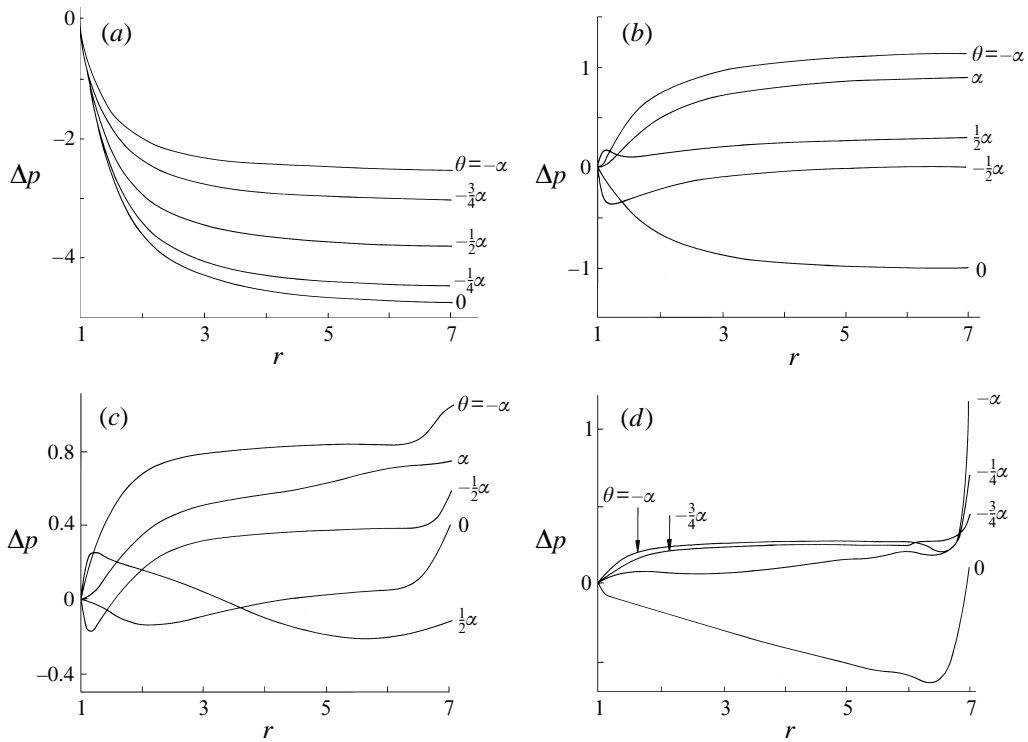


FIGURE 8. Variation of pressure, $\Delta p = p(r, \theta) - p(1, \theta)$, along the channel, at indicated values of θ for (a) half sector, $R = 5$, (b) full sector, $R = 25$, (c) full sector, $R = 50$ and (d) half sector, $R = 300$.

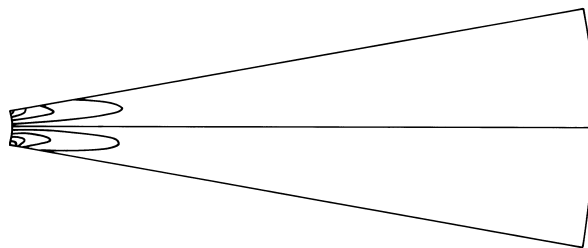


FIGURE 9. Vorticity contours for $R = 25, \alpha = \pi/18$ for flow in the full sector with the perturbation imposed at $r = r_1$.

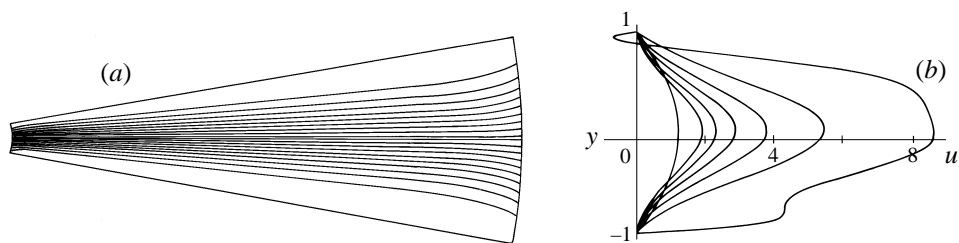


FIGURE 10. Results for $R = 25, \alpha = \pi/18$ for flow in the full sector with the perturbation imposed at $r = r_1$. (a) Streamlines for $\psi = -1 + 2n/19$ with $n = 0, 1, 2, \dots, 19$. (Note that the centreline has been shown to indicate the asymmetry.) (b) Velocity profiles at $r = 1, 2, 3, 4, 5, 6, 7$. (They can be identified by noting that the value of u on the centreline decreases with increasing r .)

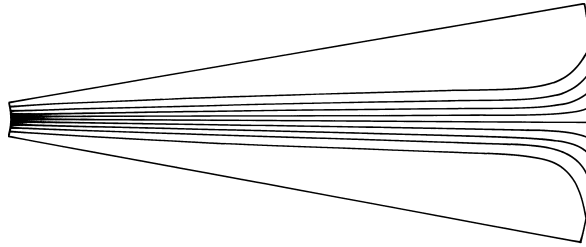


FIGURE 11. Streamlines for $R = 50, \alpha = \pi/18$ for flow in the full sector with the perturbation imposed at $r = r_2$; they are shown for $\psi = -1 + n/5$ with $n = 0, 1, 2, \dots, 10$.

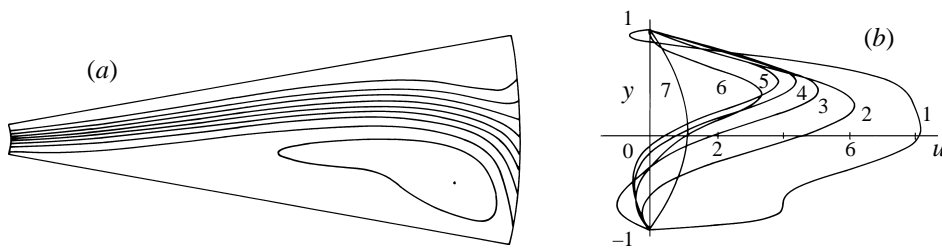


FIGURE 12. Results for $R = 50, \alpha = \pi/18$ for flow in the full sector with the perturbation imposed at $r = r_1$. (a) Streamlines for $\psi = 1 - 0.243n$ with $n = 0, 1, 2, \dots, 9$ and $\psi = -1.43$ (the minimum) indicated as a point. (b) Velocity profiles at various values of r (as indicated).

vary significantly with θ (as might be expected), and those for $\theta = 0, \pm\alpha/2, \pm\alpha$ are displayed in figure 8(c).

The solution for $R = 50$ for the full sector did not converge readily and required a large amount of computing time, so we did not proceed to larger values of R . However, for the half sector the calculations are easier, and results have been obtained up to $R = 300$.

When $R = 100$, the eddy is found even for the flow in a half sector, and again the perturbed flows due to imposing the perturbation at the inlet and the outlet are indistinguishable. Figure 13(a) shows the streamlines and the vorticity contours. Figure 13(b) shows the velocity profiles; note that there is a large re-adjustment near the outlet, where the boundary condition is imposed. Refinement of the grid is progressively more important as R increases: for example, the undulations and 'islands' in the vorticity contours near the right-hand end of the upper half of figure 13(a) are presumably due to the coarseness of the grid (which may lead to errors in the calculations or the graph plotting) because these features are exaggerated in our results (not shown here) with a coarser grid. However, the streamlines are much less affected by coarsening of the grid.

Finally, when $R = 300$, the flow in the half sector has an eddy; and the unperturbed flow in the full sector is symmetric with an eddy near each wall which is indistinguishable from an eddy in the flow in a half sector. Figure 14(a) shows the streamlines and vorticity contours, and figure 14(b) the velocity profiles. Again there is a large re-adjustment of the flow near the outlet (a consequence of the concentration of streamlines near the outlet shown in figure 14a). In figure 8(d) we show the pressure variation as a function of r for $\theta = 0, -\alpha/4, -3\alpha/4, -\alpha$. The rapid variation of the pressure near the exit is presumably a consequence of the concentration of the streamlines there.

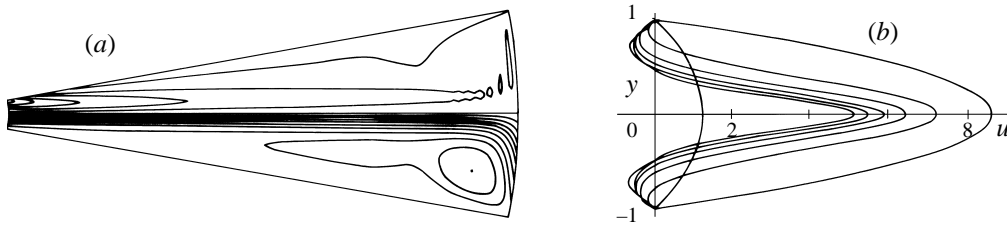


FIGURE 13. Results for $R = 100, \alpha = \pi/18$ for flow in the half sector. (a) Streamlines and vorticity contours. The streamlines, for $\psi = -0.138n$ with $n = 0, 1, 2, \dots, 9$ and $\psi = -1.378$ (the minimum) indicated as a point, are shown in the lower-half sector and vorticity contours in the upper. (b) Velocity profiles at $r = 1, 2, 3, 4, 5, 6, 7$. (They can be identified by noting that the value of u on the centreline decreases with increasing r .)

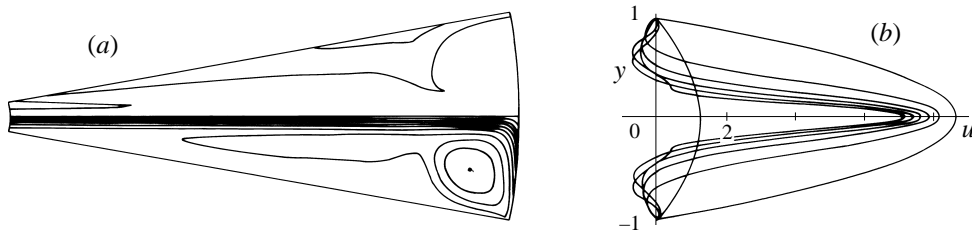


FIGURE 14. Results for $R = 300, \alpha = \pi/18$ for flow in the half sector. (a) Streamlines and vorticity contours. The streamlines, for $\psi = -0.153n$ with $n = 0, 1, 2, \dots, 9$ and $\psi = -1.53$ (the minimum) indicated as a point, are shown in the lower-half sector and vorticity contours in the upper. (b) Velocity profiles at $r = 1, 2, 3, 4, 5, 6, 7$. (They can be identified by noting that the value of u on the centreline decreases with increasing r .)

The flow patterns found for $R = 50, 100$ and 300 have led us to hazard the following conjecture. As R increases, the asymmetry of the flow in the full sector becomes more pronounced, the eddy getting larger and the rest of the flow being more narrowly confined to a thin layer near the wall on the other side, at $\theta = \alpha$ in figure 12(a). The thinness of the layer suggests that the bulk of the asymmetric flow may be calculated approximately, for large R , by allowing a slip velocity at $\theta = \alpha$; for convenience we suggest a symmetry condition precisely the same as the condition applied above at $\theta = 0$ for flow in a half sector – but applied now at $\theta = \alpha$, of course. Thus the calculation of the flow in the half sector for semi-angle 2α is used to find approximately the eddy for the asymmetric flow in the full sector with semi-angle α . In addition, the description of the flow in the full sector with semi-angle α might be completed by solving the boundary-layer problem near $\theta = \alpha$ driven by the outer flow, i.e. the slip velocity found from the problem for the half sector with semi-angle 2α .

The choice, in a theory, of boundary conditions at the inlet and outlet of a diverging sector to represent an experiment faithfully is usually difficult. Experiments are often conducted with a channel which has an inlet consisting of parallel walls long enough to establish a parabolic velocity profile, some divergent ‘test section’, and an outlet that is incompletely described.

Often in computational fluid dynamics a parabolic profile is imposed at the inlet (say, condition (2.4) with $f_1(\theta) = 3\theta(1 - \theta^2/3\alpha^2)/2\alpha$, $g_1(\theta) = 0$) and longitudinal flow at the outlet (say, condition (2.5) with appropriate f_2 and $g_2(\theta) = 0$). Now an implication of the results reported above is that if $R < R_2(\alpha)$, with a sector suitably long (depending on the size of the most significant eigenvalue), then the particular

choice of inlet and outlet conditions affects the flow little in the middle region of the sector, but if $R > R_2(\alpha)$ then the choice affects the flow substantially irrespectively of the length of the sector.

5. Conclusions

In addition to verifying a previous conjecture about the spatial development of the eigenmodes for $R = 0$, we also evaluated our computer programs by using the analytical results of JH flows as a benchmark, before we embarked on the more interesting numerical experiments. This gives confidence in the reliability of our numerical results.

The influence of the inlet and outlet of the channel has been found to be far-reaching even when the basic JH flow is spatially stable, because algebraic decay is much slower than the exponential decay which is characteristic of parallel flows, the exponential decay to which many have become accustomed. When the basic flow is spatially unstable the conditions at the inlet and outlet influence the whole flow in the channel, and it may be said that Saint-Venant's principle is invalid. It has been seen that, on the whole, the inlet conditions affect the flow more strongly and further into the interior than do the outlet conditions, whether $R < R_2(\alpha)$ or $R > R_2(\alpha)$. It is plausible that this relative importance of the inlet conditions is due to the convection of vorticity, but it seems to be a quantitative rather than a qualitative property mathematically.

The spatial modes of the linearized problem have provided a fruitful means to interpret the influence of the inlet and outlet conditions on a stable flow in the diverging channel, but it should be noted that the linearized problem is self-adjoint only when the Reynolds number is zero, and therefore that the development in space of two or more superposed modes may not be easy to predict. Indeed, by analogy with the temporal problem of superposing stable modes (cf. Gustavsson 1991; Butler & Farrell 1992; Reddy & Henningson 1993), a small perturbation of a stable JH flow at the outlet and inlet may lead to a very large perturbation of the flow in the interior of the channel when the Reynolds number is large; however, we have not observed a very strong 'transient' spatial amplification, perhaps because most of our calculations have been made for moderate values of the Reynolds number.

Note that the numerical solutions for the full sector show that when $R = 25$ the flow is nearly symmetric whereas when $R = 50$ it is clearly asymmetric. This implies that there is a pitchfork bifurcation at an intermediate value of R . The value of $R_2(\pi/18) = 28.68$ for the subcritical pitchfork bifurcation of JH flows is a plausible estimate for the value of R at the supercritical pitchfork bifurcation of this forced flow in a sector of radius ratio 7.

It has been impossible for us to simulate exactly the experiment of Nakayama (1988, figure 105) because of our ignorance of both his quantitative results and the precise conditions at the inlet and outlet of his channel, and we have shown how important those conditions are when $R > R_2(\alpha)$. Nonetheless, our attempted simulation of the experiment has been successful on the whole, even though we could not compute the asymmetric flow accurately at as large a value of the Reynolds number as 300 at which Nakayama conducted his experiment, and the calculated eddies for symmetric flow at $R = 300$ and for asymmetric flow at $R = 50$ are larger than those observed in the experiment.

Our choice of the special channel in a sector for intensive study was motivated by the need to use a prototype with which analytic and asymptotic results could be

used to interpret results of computational fluid dynamics, rather than the intrinsic engineering importance of the flow in a sector. However, we believe that the set of flows in a sector with various boundary conditions is qualitatively similar to the set of flows in a wide class of diverging channels used as diffusers, although the particular boundary conditions (2.5) are a poor model of the outlet of a diffuser.

This paper describes only two-dimensional flows in symmetric channels. The symmetry is, of course, only an idealization difficult to realize in an algorithm of computational fluid dynamics and impossible to realize in the laboratory. So the theory of imperfections is important in the practical interpretation of our results (cf. Sobey & Drazin 1986; Fearn *et al.* 1990). Also all laboratory experiments of flow in ‘two-dimensional’ channels are, of course, of three-dimensional flow. If the cross-section of the channel at each station is a rectangle, say, perhaps with a large aspect ratio to simulate a two-dimensional flow, then we may expect not only the symmetry breaking of a pitchfork bifurcation as described above, but also a pitchfork or other bifurcation to describe the symmetry breaking when a strongly three-dimensional flow first appears as the Reynolds number slowly increases.

We have treated some bifurcations of flows in a channel rather than the later stages of transition to turbulence because it is desirable to sort out the fundamentals before the more interesting, more challenging and more useful problems of flow at large values of the Reynolds number. Nonetheless, let us finally note King & Stewart’s (1991) conjecture that, as the Reynolds number R of flows in a given symmetric configuration slowly increases, first symmetry is broken and then it is recovered as the asymmetric attractors increase in size in phase space until they collide. This conjecture, if appropriately modified, seems as plausible when the configuration of the flows is asymmetric as when it is symmetric, because more than one attractor may occur at a given value of R and the domains of attraction in phase space increase in size as R becomes large. So, even though there is no exact symmetry of a channel, we may expect the flow to bifurcate and first get further from, and eventually closer to, a symmetric flow as the Reynolds number increases. One might go further and hypothesize that there is a unique attractor for flow in a given channel as R tends to infinity. There is no strong argument to justify these hypotheses but they do seem plausible descriptions of observations of flows in laboratory channels.

We are grateful to Dr I. B. Stewart for help with computer plots.

Note added in proof. Some may benefit by reading the interesting recent paper by Tutty (1996), which reports computations of steady flows in a very long channel with plane walls over most of its length.

REFERENCES

- BANKS, W. H. H., DRAZIN, P. G. & ZATURSKA, M. B. 1988 On perturbations of Jeffery–Hamel flow. *J. Fluid Mech.* **186**, 559–581.
- BATCHELOR, G. K. 1967 *An Introduction to Fluid Dynamics*. Cambridge University Press.
- BORGAS, M. S. & PEDLEY, T. J. 1990 Non-uniqueness and bifurcation in annular and planar channel flows. *J. Fluid Mech.* **214**, 229–250.
- BÜHLER, K. & KRÜCKELS, J. 1990 Strömungsformen mit Ablösung im ebenen Diffusor. *Z. Angew. Math. Mech.* **70**, T475–477.
- BUTLER, K. M. & FARRELL, B. F. 1992 Three-dimensional optimal perturbations in viscous shear flows. *Phys. Fluids A* **4**, 1637–1650.

- CLIFFE, K. A. & GREENFIELD, A. C. 1982 Some comments on laminar flow in symmetric two-dimensional channels. *Rep. TP 939*. AERE, Harwell.
- DEAN, W. R. 1934 Note on the divergent flow of fluid. *Phil. Mag. (7)* **18**, 759–777.
- DRAZIN, P. G. & REID, W. H. 1981 *Hydrodynamic Stability*. Cambridge University Press.
- FEARN, R. M., MULLIN, T. & CLIFFE, K. A. 1990 Nonlinear flow phenomena in a symmetric sudden expansion. *J. Fluid Mech.* **211**, 595–608.
- FRAENKEL, L. E. 1962 Laminar flow in symmetrical channels with slightly curved walls. I. On the Jeffery–Hamel solutions for flow between plane walls. *Proc. R. Soc. Lond. A* **267**, 119–138.
- GEORGIU, G. A. & EAGLES, P. M. 1985 The stability of flows in channels with small wall curvature. *J. Fluid Mech.* **159**, 259–287.
- GOLDSHTIK, M., HUSSAIN, F. & SHTERN, V. 1991 Symmetry breaking in vortex-source and Jeffery–Hamel flows. *J. Fluid Mech.* **232**, 521–566.
- GUSTAVSSON, L. H. 1991 Energy growth of three-dimensional disturbances in plane Poiseuille flow. *J. Fluid Mech.* **224**, 241–260.
- HAMADICHE, M., SCOTT, J. & JEANDEL, D. 1994 Temporal stability of Jeffery–Hamel flow. *J. Fluid Mech.* **268**, 71–88.
- HOOPER, A. P., DUFFY, B. R. & MOFFATT, H. K. 1982 Flow of fluid of non-uniform viscosity in converging and diverging channels. *J. Fluid Mech.* **117**, 283–304.
- KING, G. P. & STEWART, I. N. 1991 Symmetric chaos. In *Nonlinear Equations in the Applied Sciences*, (ed. W. F. Ames & C. F. Rogers), pp. 257–315. Academic.
- NAKAYAMA, Y. (Ed.) 1988 *Visualized Flow*. Pergamon.
- REDDY, S. C. & HENNINGSON, D. S. 1993 Energy growth in viscous channel flows. *J. Fluid Mech.* **252**, 209–238.
- SOBEY, I. J. & DRAZIN, P. G. 1986 Bifurcations of two-dimensional channel flows. *J. Fluid Mech.* **171**, 263–287.
- SOBEY, I. J. & MULLIN, T. 1992 Calculation of multiple solutions for the two-dimensional Navier–Stokes equations. *Proc. ICFD Conference, Reading*.
- TUTTY, O. R. 1996 Nonlinear development of flow in channels with non-parallel walls. *J. Fluid Mech.* **326**, 265–284.
- WOODS, L. C. 1954 A note on the numerical solution of fourth order differential equations. *Aero. Q.* **5**, 176–184.